Progress In Electromagnetics Research, Vol. 144, 67–78, 2014

A Method of Filtering and Unwrapping SAR Interferometric Phase Based on Nonlinear Phase Model

Haifeng Huang[1, *] and Qingsong Wang[2]

Abstract—This paper presents a new efficient algorithm of filtering and unwrapping phase images for interferometric synthetic aperture radar (InSAR) based on nonlinear phase model. First, we analyzed the statistical and signal properties of interferometric phase, and proposed the concept of nonlinear phase model. The model of reflecting topographic contour is used to approximate the interferometric phase variation occuring over the local window. And the lower amplitude bound of the principal vector is decided and the value solution method is given, which can solve effectively and adaptively the nonlinear factor of the phase. Second, we studied the application of nonlinear phase model in interferometric phase filtering. When compared with other advanced filters, the nonlinear phase compensation filter, with a higher computation efficiency and a better phase estimation accuracy in low coherence areas, has a stronger ability to reduce interferometric phase noise in rugged terrain. Finally, we introduced the nonlinear phase model to phase unwrapping, which increased the reliability of integration path and the accuracy of the phase gradient, and improved effectively the performance of phase unwrapping. And the real data processing results demonstrated the validity of the proposed nonlinear phase model and of the corresponding solutions.

1. INTRODUCTION

Interferometric synthetic aperture radar (InSAR) can fast mapping global topography with high accuracy, and the obtained data has great value [1, 2] in both military and civil applications. InSAR [3] get the information of surface 3D topography from the interferometric phase of two or more SAR complex image data gained from different perspectives as the information source. Phase filtering and phase unwrapping are two crucial steps in InSAR processing, and the performance of which will directly reduce the quality of the interferometric phase and the accuracy of the follow up products.

There is ample research on noise suppression for SAR interferometric phase. These can be divided into two categories: spatial domain filter and transform domain filter. The spatial domain filter has median filter, mean filter, adaptive filter with directionally dependent windows [4], adaptive median filter [5], the zero intermediate frequency vector filter [6], slope compensated filter [7–11], and adaptive contoured window filter [12]. Due to the circular periodic feature of the interferometric fringes, the interferometric phases will be in complex exponential form in these filters. And the transform domain filter is proposed for better performance of phase filtering. There are Fourier transform, wavelet transform, and time frequency transform. Frequency smoothing filter [13, 14], filter based on wavelet transform [15], joint subspace projection filter [16], filter based on MMSE criterion [17], and Bayesian filter [18], are mainly applied. As we know the existing phase filtering algorithms faced three major difficulties: feature preserving in dense fringe, accurate phase estimate in low coherence area, and computing speed, to which various algorithms are proposed.

The existing phase unwrapping methods can be classified into three categories: path following method, least norm method, and network flow method. The path the following method is to choose the

Received 8 August 2013, Accepted 28 November 2013, Scheduled 16 December 2013

* Corresponding author: Haifeng Huang (h_haifeng@163.com).

[1] School of Electronic Science and Engineering, National University of Defense Technology, Changsha, Hunan 410073, P. R. China.

[2] Equipment Academy of the Second Artillery Force, Beijing, P. R. China.

right integrate unwrapping path, limit the error in the noise area and avoid phase error propagations. The unwrapping techniques of which mainly include branch-cut method [19], mask-cut method [20], region growing method [21], and other improved methods. Least norm method is to convert phase unwrapping to mathematical least norm. And such methods include least square method [22], PCG method [23], and multigrid method [24]. The main idea of network flow method is the difference of the minimum unwrapped phase derivative and the wrapped phase derivative. And it has the grid minimum cost flow method [25], statistical segmentation network cost flow method [26], and maximum likelihood estimation minimum cost flow method [27]. In addition to the three algorithms, there are some other improved hybrid algorithms [28, 29]. However, the existing phase unwrapping algorithms face three major challenges in the areas of consistency, accuracy, and computing speed. Therefore some scholars have studied phase filtering and unwrapping joint processing algorithm [30–33].

By analyzing the statistical and signal properties of interferometric phase, this paper proposes the concept of nonlinear phase model and studies the phase filtering and unwrapping method based on the model. When compared with other advanced filters, the nonlinear phase compensation filter, with a higher computation efficiency and a better phase estimation accuracy in low coherence areas, has a stronger ability to reduce interferometric phase noise in rugged terrain. The model improves effectively the precision of unwrapped phase and the consistency, accuracy, and computing speed of phase unwrapping. And real data demonstrated the validity of the proposed model and of the corresponding processing method.

Here, the concept of nonlinear phase model is presented in Section 2, the phase filtering method based on the model is discussed in Section 3. Where the effectiveness of the filter is demonstrated by SIR-C/X-SAR X-band data from Mt. Etna. Section 4 studies the phase unwrapping method based on the nonlinear phase model. And the processing results of the experimental data from TerraSAR-X verified the effectiveness of the proposed method. Section 5 gives the conclusion.

2. PRESENTATION OF NONLINEAR PHASE MODEL

Due to various coherent sources, theoretical analysis of the statistical characteristics for interferometric phase is becoming more sophisticated. Just and Bamler [34] deduced the probability density function of the interferometric phase with scattering coefficients satisfying the assumption of static white circular complex Gaussian distribution. Lee [35] further studied the image intensity and the phase statistical properties of the polarization interferometric SAR. Subsequently, Lee [4] proved that the interferometric phase in the phase plane of the real data can be shown as the additive noise model, it is

$$\phi_z = \phi_x + \nu \tag{1}$$

where ϕ_z is the interferometric phase observation value, ϕ_x the interferometric phase truth value. ν is the plus noise, which is not correlated to the signal, and the mean is zero. And the variance σ_ν is a function of image looks and coherences.

Supposing that the interferometric phase over the filtering window is stationary and consistent and that the noise of each pixel is statistically independent, the larger the filtering window is, the better the filtering performance is. Spagnolini [7] and Trouvé [8, 9] presented slope compensated filter method to achieve the phase samples over the filtering window to be stationary and consistent. It assumes that the phase can be approximated by a 2D single frequency signal over a window, then

$$\psi_x(m,n) = \exp\left(j2\pi\left(mf_x + nf_y\right) + j\phi_0\right) \tag{2}$$

where $\psi_x = \exp(j\phi_x)$, (m, n) indicates the position of phase sample. (f_x, f_y) is the 2D local frequency and ϕ_0 the initial phase. The estimated value of 2D local frequency $(\hat{f}_x\ \hat{f}_y)$ is obtained by local frequency estimation, and the initial phase of center pixel (m_c, n_c) over a window is estimated by

$$\hat{\phi}_0(m_c,n_c) = \arg\left(\sum_{m=1}^{M}\sum_{n=1}^{N}\left(\psi_z(m,n)\cdot\exp\left(-j2\pi\left(m\hat{f}_x + n\hat{f}_y\right)\right)\right)\right) \tag{3}$$

where $\psi_z = \exp(j\phi_z)$, the ideal phase estimate value of pixel (m_c, n_c) is

$$\hat{\phi}_x(m_c,n_c) = 2\pi m_c\hat{f}_x + 2\pi n_c\hat{f}_y + \hat{\phi}_0(m_c,n_c) \tag{4}$$

The highly accurate result by the local frequency estimation is a critical part of the above method, which also directly determines the result of phase unwrapping. And the method assumes that the phase approximation satisfies the 2D linear phase model over a certain window. However, linear phase model compensation method has the following three problems in actual data processing: first, the phase over a certain window will no longer satisfy the linear model hypothesis in the case of strong topographic change, which will reduce phase unwrapping performance for difficult regions; second, the hypothesis limits the estimation window size that is the window could not be larger; otherwise, the phase samples over a window do not satisfy the linear model hypothesis that will lead to low computation efficiency; third, due to the larger estimation window is not allowed, then the less data samples accordingly can not effectively reduce the noise affect on the accuracy of local frequency estimates, which will lead to poor processing performance in low coherence areas.

For these concerns, the nonlinear phase model is presented to approximate the phase over the estimation window in this section. The model will use the nonlinear curved surface of reflecting topographic contour instead of a linear 2D slope to approximate the local phase over the estimation window. It assumed the interferometric phase value ϕ_x consists of two components: the nonlinear phase ϕ_p of reflecting topographic contour and the residue phase ϕ_r of reflecting terrain details, and we have

$$\phi_x = \phi_p + \phi_r \tag{5}$$

The real observed value of interferometric phase can be defined as

$$\psi_z(m,n) = \sum_{i=1}^{G} C_i \cdot \exp\left(j2\pi\left(mf_{xi} + nf_{yi}\right)\right) \tag{6}$$

where (f_{xi}, f_{yi}) is the i signal vector of 2D local frequency and G the vector numbers of signal decomposition.

Only $3G > MN$ over an estimation window (size $M \times N$), the above solution is valid. Here the total number of the unknown parameters (C_i, f_{xi}, and f_{yi}) is $3G$, and the equation numbers equal $M \times N$ samples over an estimation window.

We assume $C_1 \geq C_2 \ldots \geq C_{G_0} \ldots \geq C_G > 0$, and then the observed value of the phase can be redefined as

$$\psi_z(m,n) = \sum_{i=1}^{G_0} C_i \cdot \exp\left(j2\pi\left(mf_{xi} + nf_{yi}\right)\right) + \sum_{i=G_0+1}^{G} C_i \cdot \exp\left(j2\pi\left(mf_{xi} + nf_{yi}\right)\right) \tag{7}$$

where, $C_i \cdot \exp(j2\pi(mf_{xi} + nf_{yi}))$ ($i = 1, 2, \ldots, G_0$) is the principal vector of signal. For the weighted vector, coefficient C_i determines the weight of $C_i \cdot \exp(j2\pi(mf_{xi} + nf_{yi}))$ of the i signal for signal $\psi_z(m,n)$. Therefore, the sum phase of the principal vector can be used for the nonlinear phase ϕ_p of reflecting topographic contour

$$\phi_p = \arg\left(\sum_{i=1}^{G_0} C_i \cdot \exp\left(j2\pi\left(mf_{xi} + nf_{yi}\right)\right)\right) \tag{8}$$

And 2D Fourier transform can estimate the principal vector $C_i \cdot \exp(j2\pi(mf_{xi} + nf_{yi}))$ ($i = 1, 2, \ldots, G_0$) and the spectrum of the observed phase value. That is

$$S = \mathrm{FFT2}\left(\psi_z\right) = P \otimes \Phi = \left(\sum_{i=1}^{U \cdot V} p_i\right) \otimes \Phi = \sum_{i=1}^{U \cdot V} p_i \otimes \Phi \tag{9}$$

where $\otimes$ denotes Shur-Hadamard multiplication operation and P the spectrum complex phase matrix of the observed phase value. U, V are 2D Fourier transform points, and p_i is the power coefficient matrix of spectrum for (u_i, v_i)

$$p_i(u,v) = \begin{cases} P(u,v) & \text{if } u = u_i,\ v = v_i \\ 0 & \text{others} \end{cases} \tag{10}$$

The corresponding phase vector of the spectrum in $(u_i,\, v_i)$ is

$$\begin{aligned}\psi_i(m,n) &= \mathrm{FFT2}^{-1}(p_i \otimes \Phi) \\ &= \frac{1}{UV}\sum_{u=0}^{U-1}\sum_{v=0}^{V-1} p_i \otimes \Phi \cdot \exp\left(j2\pi m\frac{u}{U}\right)\cdot\exp\left(j2\pi n\frac{v}{V}\right) \\ &= \frac{P(u_i,v_i)}{UV}\cdot\Phi(u_i,v_i)\cdot\exp\left(j2\pi\left(m\frac{u_i}{U}+n\frac{v_i}{V}\right)\right) \end{aligned} \tag{11}$$

It can be seen that the phase of ψ_i $(i = 1,\, 2,\, \ldots,\, UV)$ equals a constant phase $\Phi(u_i,\, v_i)$ added in a 2D linear phase. Similarly, we assume $P(u_1, v_1) \geq P(u_2, v_2) \ldots \geq P(u_{G_0}, v_{G_0}) \ldots \geq P(u_{UV}, v_{UV}) \geq 0$ $(i = 1, 2, \cdots, UV)$. Then, the nonlinear phase ϕ_p of reflecting topographic contour can be estimated by

$$\begin{aligned}\hat{\phi}_p(m,n) &= \arg\left(\sum_{i=1}^{G_0}\psi_i\right) \\ &= \arg\left(\sum_{i=1}^{G_0}\frac{P(u_i,v_i)}{UV}\cdot\Phi(u_i,v_i)\cdot\exp\left(j2\pi\left(m\frac{u_i}{U}+n\frac{v_i}{V}\right)\right)\right) \\ &= \arg\left(\sum_{i=1}^{G_0}P(u_i,v_i)\cdot\Phi(u_i,v_i)\cdot\exp\left(j2\pi\left(m\frac{u_i}{U}+n\frac{v_i}{V}\right)\right)\right) \end{aligned} \tag{12}$$

When solving nonlinear phase $\hat{\phi}_p$, the equation contains a parameter G_0 to be determined. We name $P(u_{G_0},\, v_{G_0})$ the principal vector modulus lower bound. The solution of G_0 is critical, and the principal vector modulus lower bound $P(u_{G_0},\, v_{G_0})$ is too small due to the larger value, which will cause noise occurring in the estimated nonlinear phase $\hat{\phi}_p$. Then, the nonlinear phase $\hat{\phi}_p$ cannot describe the basic topographic contour.

In practice, we use the half power point of the signal frequency spectrum over a window as the principal vector modulus lower bound.

$$P(u_{G_0}, v_{G_0}) = \max(P(u,v))\Big/\sqrt{2} \quad (u,v) \in W \tag{13}$$

Since the principal vector modulus lower bound $P(u_{G_0}, v_{G_0})$ will change adaptively along the sliding estimated window, the nonlinear phase of reflecting the basic topographic contour is available.

Here, real data are applied to verify the correctness and effectiveness of the nonlinear phase model. Fig. 1(a) shows the processing results of real interferogram by SIR-C/X-SAR from the Etna volcano region.

To respectively estimate the phase over the window by linear phase model and nonlinear phase model proposed in this section, we have the results in Fig. 1(b) and Fig. 1(c). Obviously, the phase change over the window no longer satisfies linear phase model hypothesis due to the larger estimated window, while interferometric fringes estimated by nonlinear phase model have the same nature as the original phase. So, the estimated accuracy of nonlinear phase model is higher than that of linear phase model. From this, nonlinear phase model can keep greater accuracy for phase estimation over a

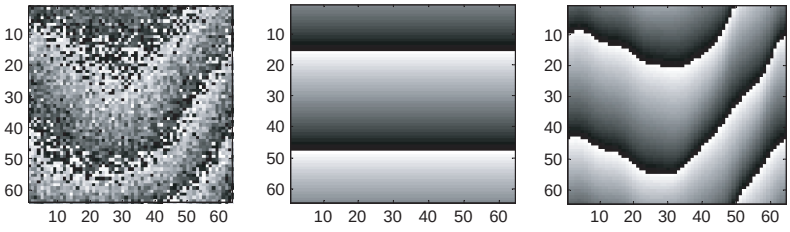

Figure 1. Estimated result of nonlinear phase component. (a) Estimated window interferogram (64×64 pixels). (b) Estimated result of linear phase model. (c) Estimated result of nonlinear phase model.

larger estimated window that reduced phase estimated time and improved data processing efficiency. Moreover, nonlinear phase model has also a good fringe estimation capability in low coherence area due to the use of a larger estimation window. And the real data processing results in Section 3 verify the validity.

3. APPLICATION OF NONLINEAR PHASE MODEL IN FILTERING

In this section, the phase filtering method based on the nonlinear phase model will be studied, by which the nonlinear phase can be batch estimated. When converting the interferometric phase with noise into frequency domain, the signal phase cannot effectively show coherent accumulation in low coherence areas. Then, the spectrum function cannot generate the distinct peaks in the frequency domain, and the scattered multi-peak phenomenon will appear. When regarding the half power point of the signal frequency spectrum over a window as the principal vector modulus lower bound, more frequency is obtained. In practice, the Fourier transform points service for border. If the number of frequencies extracted is larger than the border, the nonlinear phase is invalid. But it can be approximated by the weighted combination of nonlinear phase over the neighboring effective windows

$$\hat{\phi}_p(m,n)=\arg\left(\sum_{h=1}^{H_0}\left(\sum_{i=1}^{G_0}P_h(u_i,v_i)\cdot\Phi_h(u_i,v_i)\cdot\exp\left(j2\pi\left(m\frac{u_i}{U}+n\frac{v_i}{V}\right)\right)\right)\right) \tag{14}$$

where H_0 is the number of the neighboring effective windows. Because of noise and model approximation, the nonlinear phase between the blocks may not be continuous. We have the following against the discontinuities:

(1) Processing nonlinear phase estimation can cause interferometric phase data to block. There is some overlap between the sub-block windows. And the overlap is not more than half the size of the window. To improve the efficiency of Fourier transform, generally the data block size is of two integer powers.

(2) When the principal vector is estimated in the block window created above, it would be 2D weighted that can further weaken the discontinuity. And the weighting matrix is as follows:

$$W_V=(I_xK_x)\otimes(K_yI_y) \tag{15}$$

where I_x is M_e dimensional unit column vector, I_y the N_e dimensional unit row vector, and M_e and N_e denote the estimated window size of nonlinear phase. K_x is dimensional unit row vector, K_y is M_e dimensional unit column vector.

$$K_x=\left[0,\frac{2}{N_e},\ldots,\frac{N_e-4}{N_e},\frac{N_e-2}{N_e},\frac{N_e-2}{N_e},\frac{N_e-4}{N_e},\ldots,\frac{2}{N_e},0\right] \tag{16}$$

$$K_y=\left[0,\frac{2}{M_e},\ldots,\frac{M_e-4}{M_e},\frac{M_e-2}{M_e},\frac{M_e-2}{M_e},\frac{M_e-4}{M_e},\ldots,\frac{2}{M_e},0\right] \tag{17}$$

(3) After adding all principal vectors, which is 2D weighted, the nonlinear phase $\hat{\phi}_p$ can be estimated according to Equation (12).

After removing the nonlinear phase from the original interferometric phase, the remaining over the filtering window is basically the same size, and the noise phase in each pixel is statically independent. Therefore, just a simple multi-look filter is needed to average noise. Then, the estimated value of interferometric phase for the center pixel can be computed as follows

$$\hat{\phi}_x(m_{fc},n_{fc})=\arg\left(\sum_{m_f=1}^{M_f}\sum_{n_f=1}^{N_f}\left(\psi_z(m_f,n_f)\cdot\exp\left(-j\hat{\phi}_p(m_f,n_f)\right)\right)\right)+\hat{\phi}_p(m_{fc},n_{fc}) \tag{18}$$

where M_f and N_f are the size of the filtering window.

Note that if the principal vector modulus lower bound $P(u_{G_0},v_{G_0})=\max(P(u,v))$, the proposed filter is equivalent to the slope compensated filter and if $P(u_{G_0},v_{G_0})>\max(|P(u,v)|)$, then the proposed filter is equivalent to the mean filter.

The interferogram of the real data by SIR-C/X-SAR from Etna Volcano of Italy confirmed the effectiveness of the proposed method. We also made a comparison between Lee filter [4], slope

compensated filter [10], adaptive contoured window filter [12], joint subspace projection filter [16], and the proposed filter. In order for easy comparative analysis, the filtering results are removed by the same plain phase, and the most complicated local area (crater region contains 400×300 pixels) chosen from all interferometric phase is presented. Fig. 2(a) is the original interferometric phase, and the fringes of the entire region are not very clear, in which there are more serious noise and a large number of residues.

The result by Lee filter is shown in Fig. 2(b). Due to strong noise, the Lee filter cannot choose the right directional dependent window so that the filtering quality is poor. Particularly in the highly dense fringes, the fringe feature is failure. The result by slope compensated filter is shown in Fig. 2(c). The filtering quality with the estimated local frequency and the compensated slope phase is better than that of Lee filter. Due to the small estimated window, the filtering performance is degraded in low coherence region. The result by adaptive contoured window filter is shown in Fig. 2(d). The contour window cannot be effectively created due to strong noise, so the fringe is distorted. The result by joint subspace projection filter is shown in Fig. 2(e). The fringe of the whole region is very clear, but too

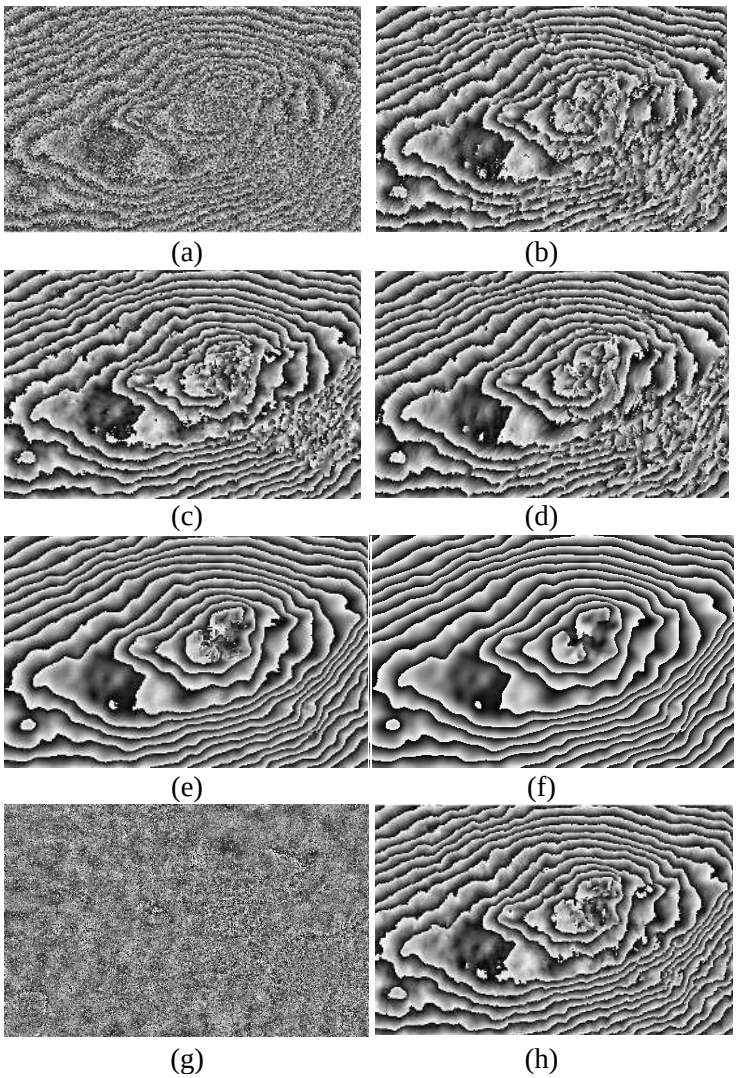

Figure 2. Performance comparison of filters: (a) the original interferometric phase of Etna crater; (b) the result of Lee filter; (c) the result of slope compensated filter*; (d) the result of adaptive contoured window filter*; (e) the result of joint subspace projection filter*; (f) the nonlinear phase estimated by the proposed method; (g) the residue phase; (h) the result of the proposed filter. *Note: the results of Figs. 2(c)–(e) and the following computing speed are provided by the corresponding authors of reference [10, 12, 16].

smooth to lose some of the terrain details. Then, it depends on the noise subspace dimension, if too large or too small, there will be over filtering or less filtering. Besides, this method is of highly intensive computation and time consuming.

The results by the proposed filter are shown in Figs. 2(f)–(h). The nonlinear phase estimation window size is $32 * 32$, and the filtering window size is $5 * 5$. Comparing the filtering result with the original noisy phase and other four filtering results, we found the noise is significantly reduced and the fringes are much better preserved. The filtering performance is shown in Table 1, in which there are the residual points statistics of original interferometric phase and the results of various filters. The proposed filter reduced drastically the number of residues by 99% with a $5 * 5$ filtering window, and maintained effectively the fringe feature and the topographical details. Although the Joint subspace projection filter had the least number of residues, it lost some of the terrain details.

Table 1. The residual points statistics.

Original interferometric phase	Lee filter	Slope-compensated filter	Adaptive contoured window filter	Joint subspace projection filter	The proposed filter
20806	2641	853	1119	86	194

Furthermore, the proposed method is extremely fast. For full Mount Etna data ($1024 * 1024$ pixels) mentioned earlier, the time expense is shown in Table 2.

Table 2. The time expense statistics.

Multi-look mean filter	Lee filter	Slope-compensated filter	Adaptive contoured window filter	Joint subspace projection filter	The proposed filter
3.9 s (P4 CPU 2.4 GHz)	48.9 s (P4 CPU 2.4 GHz)	15 s (CPU 3.4 GHz)	25.6 s (CPU 2.8 GHz)	5031 s (Dual core CPU 2.5 GHz)	6.1 s (P4 CPU 2.4 GHz)

We can see the proposed filter is faster and more effective than the other advanced filters,

At present, European Space Agency (ESA), Jet Propulsion Laboratory (JPL), and German Space Agency (DLR) and other research institutions applied the multi-look mean filter for filtering in InSAR data processing software. As we know, mean filter is chosen for the simple and fast characteristic. Therefore, method of high performance and fast filtering in the actual InSAR data processing, has a practical significance. And in the future, the proposed fast filtering method with high performance may be able to play an important role in processing massive data obtained by global InSAR mapping.

4. APPLICATION OF NONLINEAR PHASE MODEL IN UNWRAPPING

In the previous section, we first analyzed linear phase model and its deficiency, then proposed nonlinear phase model and verified its effectiveness. In this section, we will introduce the nonlinear phase model to phase unwrapping for path following method.

The phase obtained by interferometry is a wrapped one. The value solution range of the phase is in the principal value interval $(-\pi, \pi]$, but there is a difference $2n\pi$ (n for integer) occurred in the required real phase. The purpose of phase unwrapping is to solve phase wrapping, and get a basic successive phase surface. Phase unwrapping for path following method has two steps. First, estimate unwrapped phase differences between neighboring pixels. Second, integrate with the estimated phase gradient along the right path. And path following method has branch-cut algorithm and region-growing algorithm. The former is to correctly achieve the branch cutting and prevent the passing of integration path by

identifying residues, and avoid phase error propagation in the entire phase image. The latter is guided by a quality map. It performs unwrapping from a high quality area to a low quality area gradually, so that the error propagation is limited to the low quality area.

There are two key factors to determine the unwrapping performance for path following method: first, choose the right integration path. Second, estimate the accurate integrate phase gradient. Since the estimated nonlinear phase reflects topographic contour, the application of nonlinear phase model then can effectively improve the correctness of integration path and the accuracy of phase gradient. The following discussed how to use the nonlinear phase model to improve the unwrapping performance for branch-cut algorithm and region-growing algorithm.

Branch-cut method [19] connects neighboring residues to achieve the best branch cutting by identifying residues, then determines the integration path, and prevents error propagation along the integration path. Branch cutting is extremely important for branch-cut method; if set incorrectly, it will affect the speed and accuracy of phase unwrapping. And the distribution of residues determines the setting. There are two applications of nonlinear phase in unwrapping for branch-cut method.

(1) Branch cutting is no longer determined by the residual distribution of original phase, but by that of nonlinear phase which also determines the integration path.

(2) Phase unwrapping along the integration path is

$$\phi_u = \hat{\phi}_{p0} + \sum_{i \in l} \Delta\hat{\phi}_{pi} + \arg\left\{\exp\left(j\left(\phi - \hat{\phi}_p\right)\right)\right\} \tag{19}$$

where ϕ is the wrapped phase of the current unwrapping pixel, $\hat{\phi}_p$ the estimated nonlinear phase, $\hat{\phi}_{p0}$ the value of nonlinear phase at the starting pixel of the integration path l. $\Delta\hat{\phi}_{pi} = \arg\{\exp(j(\hat{\phi}_{pi} - \hat{\phi}_{pi-1}))\}$ is the gradient of nonlinear phase along the integration path.

For the two aspects, branch-cut method can effectively shorten the length of branch cutting and improve the unwrapping efficiency. And the unwrapping phase gradient based on nonlinear phase is obtained, still a more reliable unwrapping path and the gradient of integration phase are available at low coherence area.

Region-growing algorithm [21] is another unwrapping method of path following has two steps: region division and region unwrapping. Refer to the phase quality map (coherence map, pseudo coherence map, etc.), region division is to divide and sort the images into different quality regions. The obtained result will determine the phase unwrapping path. And region unwrapping is from high quality area to low quality area. The unwrapping phase data from different directions is used to achieve phase unwrapping for the current growth pixel, which is helpful to reduce the error effect from a single prediction direction. Similarly, there are two aspects for region-growing algorithm to introduce nonlinear phase to phase unwrapping.

(1) We use the following measure function as a quality standard in region division:

$$Q = \left|E\left\{\exp\left(j\hat{\phi}_p\right)\right\}\right| \tag{20}$$

where $||$ denotes modulo operation, $E\{\}$ the expectation value, and $\hat{\phi}_p$ the estimated nonlinear phase.

(2) The solution of region unwrapping is

$$\phi_u = \hat{\phi}_p + 2\pi \cdot \mathrm{int}\left(\frac{\phi^p - \hat{\phi}_p}{2\pi}\right) + \arg\left\{\exp\left(j\left(\phi - \hat{\phi}_p\right)\right)\right\} \tag{21}$$

Here, ϕ is the wrapped phase of the current growth pixel, and ϕ^p the unwrapping estimation of the corresponding current growth pixel based on nonlinear phase. It is

$$\phi^p = \left(\sum_{k=1}^{N_u} \omega_k \phi_k^p\right) \Big/ \left(\sum_{k=1}^{N_u} \omega_k\right) \tag{22}$$

N_u denotes the number of unwrapping estimation determined by the already unwrapping pixels. When a prediction direction has two unwrapping pixels, $\omega_k = 1$, $\phi_k^p = 2\hat{\phi}_p[k] - \hat{\phi}_p[k']$. And when it has only one unwrapping pixel, $\omega_k = 0.5$, $\phi_k^p = \hat{\phi}_p[k]$.

For the above two improvements, the blocks of region division will be reduced, and the estimation reliability of phase unwrapping will be enhanced.

From this, we find that the introduction of nonlinear phase can effectively improve the unwrapping performance. And the nonlinear phase of reflecting topographic contour improved the reliability of the integration path and the accuracy of the phase gradient. The effectiveness of the modified method is verified by processing the real data. Fig. 3(a) is the magnitude image obtained by TerraSAR-X spotlight mode. The area is divided into three blocks by a "Y" shaped cross road.

The unwrapping result of the upper right side in Fig. 3(c) is discontinuous with the other two blocks, and the error of the road area is obvious. Similarly, in Fig. 3(e) the unwrapping result of the lower right corner is discontinuous with the other two blocks. Compared with the previous method, the unwrapping performance of the modified method in Fig. 3(d) and Fig. 3(f) is significantly improved. It is possible to correctly estimate the ambiguity number of phase for the road area, even the regions that fail to unwrap do not exist in the unwrapping results. To compare more clearly the unwrapping performance of the two methods before and after improvement, Fig. 4 shows unwrapping results in range and azimuth for the neighborhood of the three-way intersection (red thread in Fig. 3(b)). We found from Fig. 4 that the branch-cut method or the region-growing method cannot get a correct unwrapping path due to the effect of phase noise at low-coherence area of the road. And the accurate ambiguity number of phase unwrapping is not available for road area; then the discontinuity (an integer times difference of 2π) between the blocks occurs in the unwrapping results. While the correct and effective unwrapped results can be obtained after improvement of the two unwrapping methods by introducing nonlinear phase. And the right ambiguity number of the road area is available, still the continuity of phase-unwrapping results is better than that of before improvement.

Note that the time expense of unwrapping the data mentioned above by branch-cut method and

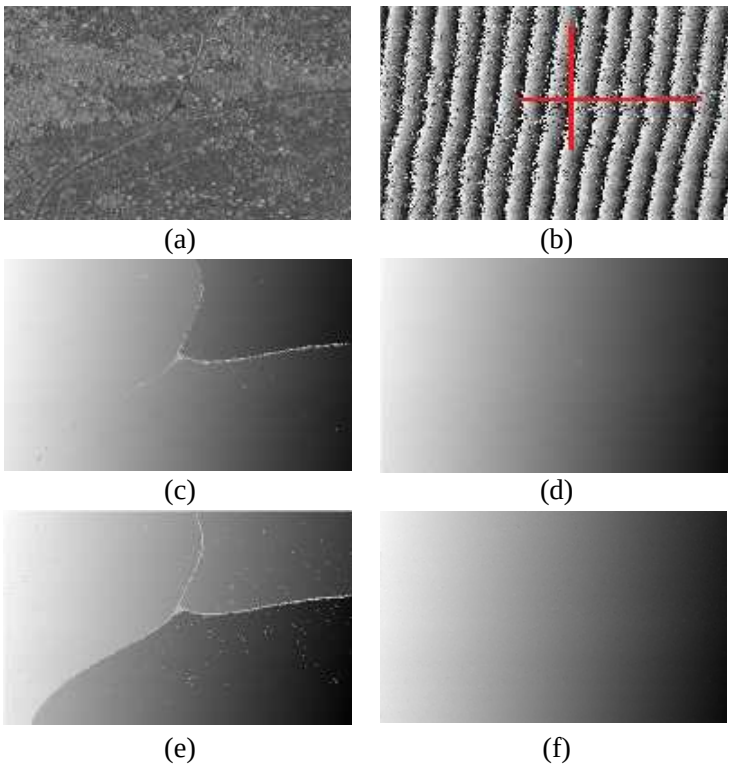

Figure 3. Comparison of unwrapping performance. (a) The magnitude image by TerraSAR-X spotlight. (b) Phase before unwrapping. (c) Phase unwrapping result by branch-cut method. (d) Phase unwrapping result of the modified branch-cut method by introducing nonlinear phase. (e) Phase unwrapping result by region-growing method. (f) Phase unwrapping result of the modified region-growing method by introducing nonlinear phase.

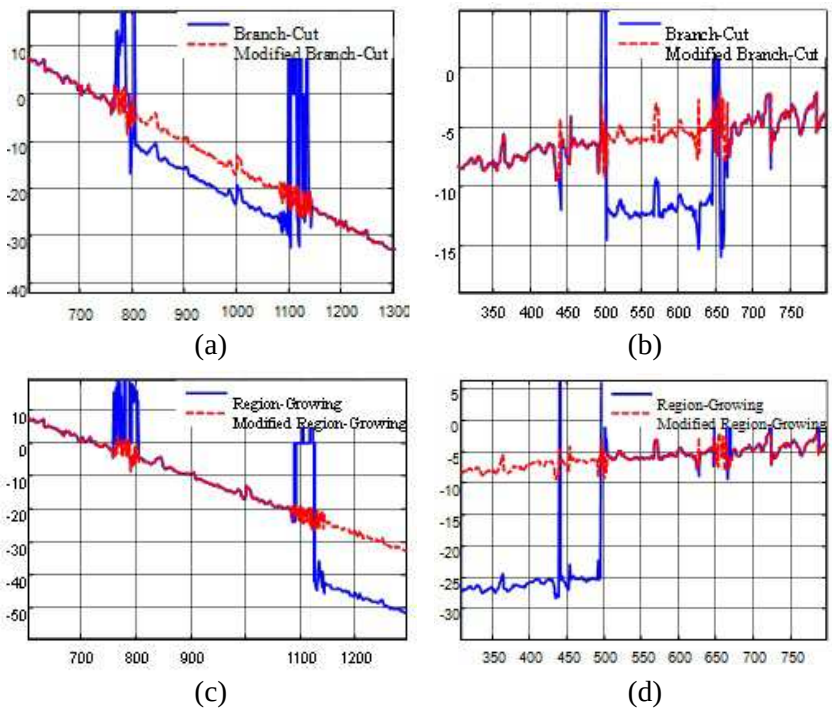

Figure 4. Comparison of unwrapping results. (a) Comparison of unwrapping results in range for branch-cut method. (b) Comparison of unwrapping results in azimuth for branch-cut method. (c) Comparison of unwrapping results in range for region-growing method. (d) Comparison of unwrapping results in azimuth for region-growing method.

region-growing method are 21.4 s and 19.3 s respectively, and the estimated time of the nonlinear phase is 3.2 s. From that, the proposed method improved obviously the unwrapping performance with less increased time expense.

5. CONCLUSIONS

Phase filtering and unwrapping are two key steps in InSAR processing, and the performance of which will directly affect the accuracy of later productions. This paper studied on this subject based on this understanding. First, by analyzing the statistical and signal characteristics of interferometric phase, the concept of nonlinear phase model is proposed. It uses the nonlinear phase model of reflecting the topographic contour to approximate the phase change appearing over the local window. And we have given out the adaptive extraction method of nonlinear phase. Then, the paper discussed the phase filtering and unwrapping method based on the nonlinear phase model. Compared with other advanced filters, nonlinear phase compensation filter with a better phase estimation accuracy in low coherence areas and a higher computation efficiency, has a stronger ability to reduce interferometric phase noise in rugged terrain. The effectiveness of the proposed filter is demonstrated by SIR-C/X-SAR X-band data of Mt. Etna. The application of nonlinear phase model for phase unwrapping improved effectively the precision of unwrapped phase and the consistency, accuracy, and computing speed of phase unwrapping. And the processing results of real data by TerraSAR-X verified the effectiveness of the proposed method.

ACKNOWLEDGMENT

The authors would like to thank Professor Daiyin Zhu of Nanjing University of Aeronautics and Astronautics, Professor Zhenfang Li of Xidian University, and Professor Qifeng Yu of National University of Defense Technology and academician of Chinese Academy of Sciences, which provided data processing

results by their own methods. This work is supported by the National Natural Science Foundation of China (Grant No. 61002031). Thanks are also given to the German Aerospace Center (DLR) and the Infoterra Company for providing the data by SIR-C/X-SAR and TerraSAR-X.

REFERENCES

1. Krieger, G., A. Moreira, H. Fiedler, et al., "TanDEM-X: A satellite formation for high-resolution SAR interferometry," *IEEE Transactions on Geoscience and Remote Sensing*, Vol. 45, 3317–3341, Nov. 2007.
2. Farr, T. G., S. Hensley, E. Rodriguez, et al. "The shuttle radar topography mission," *CEOS SAR Workshop*, 361–363, 2000.
3. Bamler, R. and P. Hartl, "Synthetic aperture radar interferometry," *Inverse Problems*, Vol. 14, R1–R54, 1998.
4. Lee, J. S. and K. P. Papathanassiou, "A new technique for noise filtering of SAR interferometric phase images," *IEEE Transactions on Geoscience and Remote Sensing*, Vol. 36, No. 5, 1456–1465, Sep. 1998.
5. Liao, M.-S., H. Lin, Z.-X. Zhang, et al., "Adaptive algorithm for filtering interferometric phase noise," *Journal of Remote Sensing*, Vol. 7, No. 2, 98–105, 2003.
6. Jin. G.-W., Q. Xu, Y. Zhang, et al., "The zero intermediate frequency vector filtering for interferograms," *Acta Geodaetica et Cartographica Sinica*, Vol. 35, No. 1, 24–29, 2006.
7. Spagnolini, U., "2-D phase unwrapping and instantaneous frequency estimation," *IEEE Transactions on Geoscience and Remote Sensing*, Vol. 33, No. 3, 579–589, 1995.
8. Trouvé, E., M. Caramma, and H. Maitre, "Fringe detection in noisy complex interferograms," *Appl. Opt.*, Vol. 35, No. 20, 3799–3806, 1996.
9. Trouvé, E., J. M. Nicolas, and H. Maitre, "Improving phase unwrapping techniques by the use of local frequency estimates," *IEEE Transactions on Geoscience and Remote Sensing*, Vol. 36, No. 6, 1963–1972, 1998.
10. Zhu, D.-Y., Z.-D. Zhu, and Q.-C. Xie, "A topography adaptive interferogram filter based on local frequency estimation," *Acta Electronica Sinica*, Vol. 30, No. 12, 1853–1856, Dec. 2002.
11. Cai, B., D. Liang, and Z. Dong, "A new adaptive multiresolution noise filtering approach for SAR interferometric phase images," *IEEE Geoscience and Remote Sensing Letters*, Vol. 5, No. 2, 266–270, 2008.
12. Yu, Q., X. Yang, S. Fu, et al., "An adaptive contoured window filter for interferometric synthetic aperture radar," *IEEE Geoscience and Remote Sensing Letters*, Vol. 4, No. 1, 23–26, 2007.
13. Goldstein, R. M. and C. L. Werner, "Radar interferogram filtering for geophysical applications," *Geophys. Res. Lett.*, Vol. 25, No. 21, 4035–4038, 1998.
14. Baran, I., M. P. Stewart, B. M. Kampes, et al., "A modification to the Goldstein radar interferogram filter," *IEEE Transactions on Geoscience and Remote Sensing*, Vol. 41, No. 9, 2114–2118, 2003.
15. Lòpez, C., X. Fàbregas, O. J. Mallorquì, et al., "Noise filtering of SAR interferometric phase based on wavelet transform," *IEEE Proceeding of 2001 International Geoscience and Remote Sensing Symposium*, Vol. 6, 2928–2930, Sydney, Australia, 2001.
16. Li, Z., Z. Bao, H. Li, et al., "Image auto-coregistration and InSAR interferogram estimation using joint subspace projection," *IEEE Transactions on Geoscience and Remote Sensing*, Vol. 44, No. 2, 288–297, 2006.
17. Li, H. and G. Liao, "An estimation method for InSAR interferometric phase based on MMSE criterion," *IEEE Transactions on Geoscience and Remote Sensing*, Vol. 48, No. 3, 1457–1469, Mar. 2010.
18. Ferraiuolo, G. and, G. Poggi, "A Bayesian filtering technique for SAR interferometric phase fields," *IEEE Trans. Image Process.*, Vol. 13, No. 10, 1368–1378, 2004.
19. Goldstein, R. M., H. A. Zebker, and C. L. Werner, "Satellite radar interferometry two dimensional phase unwrapping," *Radio Science*, Vol. 23, No. 24, 713–720, 1988

20. Flynn, T. J., "Consistent 2-D phase unwrapping guided by a quality map," *IEEE Proceeding of 1996 International Geoscience and Remote Sensing Symposium*, Vol. 4, 2057–2059, 1996.
21. Xu, W. and I. Cumming, "A region-growing algorithm for InSAR phase unwrapping," *IEEE Transactions on Geoscience and Remote Sensing*, Vol. 37, No. 1, 124–134, Jan. 1999.
22. Pritt, M. D. and J. S. Shipman, "Least squares two dimensional phase unwrapping using FFT," *IEEE Transactions on Geoscience and Remote Sensing*, Vol. 32, No. 3, 704–708, 1994
23. Ghiglia, D. C. and M. D. Pritt, *Two Dimensional Phase Unwrapping: Theory, Algorithms, and Software,* John Wiley & Sons, New York, 1998.
24. Pritt, M. D., "Phase unwrapping by means of multi-grid techniques for interferometric SAR," *IEEE Transactions on Geoscience and Remote Sensing*, Vol. 34, No. 3, 728–738, 1996.
25. Costantini, M., "A novel phase unwrapping method based on network programming," *IEEE Transactions on Geoscience and Remote Sensing*, Vol. 36, No. 3, 813–831, 1998
26. Chen, C. W. and H. A. Zebker, "Phase unwrapping for large SAR interferograms: Statistical segmentation and generalized network models," *IEEE Transactions on Geoscience and Remote Sensing*, Vol. 40, No. 8, 1709–1719, 2002
27. Lachaise, M. and R. Bamler, "Minimum cost flow phase unwrapping supported by multibaseline unwrapped gradient," *Proceedings of European Conference on Synthetic Aperture Radar, EUSAR 2010*, 16–19, Germany, 2010.
28. Xiong, T., Y. Chen, J. Yang, et al., "Phase unwrapping method based on the phase change technology," *Science China Information Sciences*, Vol. 40, No. 3, 445–457, 2010.
29. Wang, Z. and Y. Yuan, "A combination of the phase unwrapping algorithm of InSAR data," *Progress in Natural Science*, Vol. 18, No. 7, 833–835, 2008.
30. Martinez Espla, J. J., T. Martinez-Marin, and J. M. Lopez-Sanchez, "Using a grid-based filter to solve InSAR phase unwrapping," *IEEE Geoscience and Remote Sensing Letters*, Vol. 5, No. 2, 147–151, Apr. 2008.
31. Suksmono, A. B. and A. Hirose, "Adaptive noise reduction of InSAR images based on a complex-valued MRF model and its application to phase unwrapping problem," *IEEE Transactions on Geoscience and Remote Sensing*, Vol. 40, No. 3, 699–709, Mar. 2002.
32. Otmar, L., H. Nies, S. Knedlik, et al., "Phase unwrapping for SAR interferometry — A data fusion approach by Kalman filtering," *IEEE Transactions on Geoscience and Remote Sensing*, Vol. 46, No. 1, 47–58, Jan.2008.
33. Li, Z., B. Zheng, and Z. Suo, "A joint image coregistration, phase noise suppression, and phase unwrapping method based on subspace projection for multibaseline InSAR systems," *IEEE Transactions on Geoscience and Remote Sensing*, Vol. 45, No. 3, 584–591, Mar. 2007.
34. Just, D. and R. Bamler, "Phase statistics of interferograms with application to synthetic aperture radar," *Appl. Opt.*, Vol. 33, No. 20, 4361–4368, 1994.
35. Lee, J. S., K. W. Hoppel, and S. A. Mango, "Intensity and phase statistics of multilook polarimetric and interferometric SAR imagery," *IEEE Transactions on Geoscience and Remote Sensing*, Vol. 32, No. 5, 1017–1027, 1994.